RECENT RESULTS IN THE INFRARED SECTOR OF QCD*

D. Binosi

European Centre for Theoretical Studies in Nuclear Physics
and Related Areas (ECT*)
and
Fondazione Bruno Kessler
Villa Tambosi, Strada delle Tabarelle 286, 38123 Villazzano (TN), Italy

(Received September 17, 2012)

We review the most recent results, derived within the combined framework of the pinch technique and the background field method, describing certain QCD nonperturbative properties.

DOI:10.5506/APhysPolBSupp.5.993
PACS numbers: 12.38.Aw, 12.38.Lg, 14.70.Dj

Since its introduction, the combined framework of the pinch technique (PT) [1–5] and the background field method [6], known in the literature as the PT-BFM scheme [7–9], has provided a sound theoretical basis for addressing the nonperturbative study of the QCD Green's functions of both the gluon as well as the ghost sector of QCD, respecting at the same time the fundamental symmetries of the theory. Results derived within this framework include, but are not limited to, the first evidence of the existence (in the Landau gauge) of massive solutions in the properly truncated QCD Schwinger–Dyson equations (SDEs) as found in lattice simulations [10] and which can be interpreted in terms of a nonperturbative mass [10–12] which tames the infrared (IR) divergences of the Green's functions of the theory, the study of the Kugo–Ojima function [13] and the identification of the role of the ghost for achieving a chiral symmetry breaking pattern that provides for dynamically generated quark masses compatible with phenomenology [14].

In this paper, I will present the latest results derived within the PT-BFM framework (in the Landau gauge) and discuss in particular:

* Presented at the Workshop "Excited QCD 2012", Peniche, Portugal, May 6–12, 2012.

- the use of the SDEs to compute the nonperturbative modifications caused to the IR finite gluon propagator by the inclusion of a small number of quark families [15];
- the general derivation of the full nonperturbative equation that governs the momentum evolution of the dynamically generated gluon mass [16].

1. Unquenching the gluon propagator

As described in [15], the PT-BFM allows to develop an approximate method for "unquenching" the (IR finite) gluon propagator, computing nonperturbatively the effects induced by a small number of light quark families. The procedure consists of two basic steps:

- computing the fully-dressed quark-loop diagram, using as input the nonperturbative quark propagators obtained from the solution of the gap equation, together with an Ansatz for the fully-dressed quark-gluon vertex that preserves gauge-invariance [14];
- adding this result to the quenched gluon propagator obtained in large-volume lattice simulations.

The key assumption of the method sketched above is, therefore, that the effects of a small number of quark families to the gluon propagator may be considered as a "perturbation" to the quenched case, of which the quark-loop diagram constitutes the leading correction term, with the subleading terms stemming from the (originally) pure Yang–Mills diagrams which now get modified from the quark loops nested inside them. Thus, within the approximations we will employ, these latter corrections are neglected, so that one can identify (even when dynamical quarks are present) with the quenched lattice propagator all SDE graphs except the quark loop diagram.

The expression for the PT-BFM scalar cofactor $\Delta_Q(q^2)$ of the unquenched propagator (the subindex Q standing for "quarks"), defined as $\Delta_Q^{\mu\nu}(q) = P_{\mu\nu}(q)\Delta_Q(q^2)$ with $P_{\mu\nu} = g_{\mu\nu} - q_\mu q_\nu/q^2$ the dimensionless transverse projector, can be then written as [15]

$$\Delta_Q\left(q^2\right) = \frac{\Delta\left(q^2\right)}{1 + \left\{i\,\widehat{X}\left(q^2\right)\left[1 + G\left(q^2\right)\right]^{-2} - \lambda^2\right\}\Delta\left(q^2\right)}\,. \tag{1}$$

In what follows, we will describe all the different terms appearing in the right-hand side of the formula above.

- $\Delta(q^2)$ is the quenched propagator which, as already pointed out, will be identified with the one obtained from the large volume lattice simulations.

- $G(q^2)$ is a special Green's function particular to the PT-BFM which achieves the conversion from the PT-BFM to the conventional gluon propagator [8, 9]; in the Landau gauge it is known to coincide with the Kugo–Ojima function [13, 17].

- $\widehat{X}(q^2)$ is the PT-BFM scalar cofactor resulting from the calculation of the quark loop diagram; defining $\widehat{X}_{\mu\nu}(q) = P_{\mu\nu}(q)\widehat{X}(q^2)$, one has

$$\widehat{X}\left(q^2\right) = -\frac{g^2}{12}\int\limits_k \mathrm{Tr}\left[\gamma^\mu S(k)\widehat{\Gamma}_\mu(k+q,-k,-q)S(k+q)\right], \qquad (2)$$

  where S is the full fermion propagator (with $S^{-1}(p) = -iA(p)[\not{p} - \mathcal{M}(p)]$ and $\mathcal{M}$ the dynamical quark mass), and $\widehat{\Gamma}_\nu$ is the full PT-BFM quark-gluon vertex. To evaluate expression (2) one proceeds as follows: *(i)* the nonperturbative behavior of the functions A and $\mathcal{M}$ appearing in the definition of the full quark propagator is obtained by solving numerically the quark gap equation as done in [14]; *(ii)* for the full PT-BFM quark-gluon vertex $\widehat{\Gamma}$ one uses a suitable nonperturbative Ansatz, satisfying the gauge symmetry of the theory — such as the Ball–Chiu vertex [18] or the Curtis–Pennington vertex [19] — improved with the inclusion of the (numerically crucial) dependence on the ghost dressing function and the quark-ghost scattering amplitude [14]. To be sure, other forms of the quark-gluon vertex exists, such as those reported in [20, 21], and it would be interesting to check what effects they might have on our predictions.

- Finally, $\lambda^2 = \Delta_Q^{-1}(0) - \Delta^{-1}(0) \equiv m_Q^2(0) - m^2(0)$ denotes the gluon mass difference at $q^2 = 0$ (notice that since $\widehat{X}(0) = 0$, the quark contribution to this quantity is only indirect, *i.e.* through the modification it will induce on the various ingredients appearing in the mass equation — see the next section). A solid first-principle determination of λ^2 has not been attempted, mainly due to the fact that the derivation of the *complete* mass equation has been only very recently achieved [16] (see the next section again); in the analysis presented here, we will restrict ourselves to extracting an approximate range for λ^2, by employing a suitable extrapolation of the (unquenched) curves obtained from intermediate momenta towards the deep IR.

The main results of our study may be summarized as follows (see Fig. 1). The basic effect of the quark loop(s) (one or two families with a constituent mass of the order of 300 MeV) is to suppress considerably the gluon propagator in the IR and intermediate momenta regions, while the ultraviolet

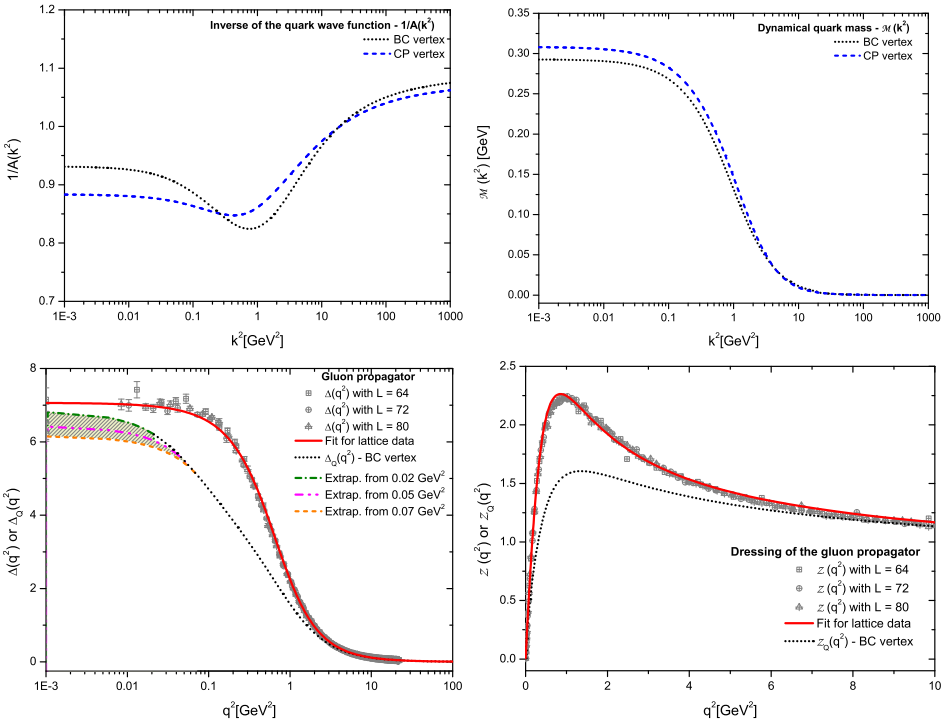


Fig. 1. Top panels: Solution of the quark gap equation: $A^{-1}(k^2)$ (left) and dynamical quark mass $\mathcal{M}(k^2)$ (right) renormalized at $\mu = 4.3$ GeV; dotted (black) curves correspond to the improved Ball–Chiu vertex, while dashed (blue) curves to the improved CP vertex. Bottom panels: Comparison between the quenched and the unquenched gluon propagator (left) and dressing function (right). The shaded striped region of the left plot shows the possible values that $\Delta_Q(0)$ can assume at zero momentum depending on the extrapolation point used; in the case of the dressing function (which is basically insensible to the IR saturation point), we used a curve with an extrapolation point at $q^2 = 0.05$ GeV^2. The quenched lattice results of [22] are also displayed for comparison.

tails increase, exactly as expected from the standard renormalization group analysis. In addition, the inclusion of light quarks makes the gluon propagator saturate at a lower point, which can be translated into having a larger gluon mass. As far as the gluon dressing function $\mathcal{Z}(q^2) = q^2\Delta(q^2)$ is concerned, one observes a suppression of the intermediate momentum region peak. A comparison with the recent full QCD lattice simulations of [23] is currently underway; however, a comparison with some of the available lattice data [24] (Fig. 2) shows an excellent qualitative agreement as well as a rather favorable quantitative agreement (with discrepancies at the 20% level maximum).

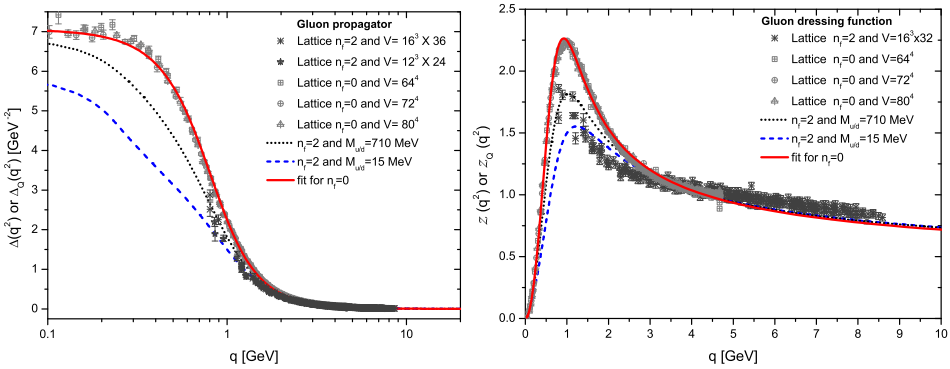


Fig. 2. The unquenched gluon propagator (left) and dressing function (right) obtained in [24] (dark gray stars), together with the SDE results for two light quarks with $M_{u/d} = 15$ MeV (dashed (blue) curve) and $M_{u/d} = 710$ MeV (dotted (black) curve). Quenched data [22] are again shown for comparison.

2. The complete gluon mass equation

Massive solutions of the gluon propagator SDE can be parametrized as (Euclidean space) $\Delta^{-1}(q^2) = q^2 J(q^2) + m^2(q^2)$; therefore, one faces the fundamental question of how to disentangle from the SDE the part that determines the evolution of the mass $m^2(q^2)$ from the part that controls the evolution of the "kinetic" term $J(q^2)$. This is to be contrasted to what happens in the analogous studies of chiral symmetry breaking, where one derives a system of two coupled equations, one determining the "wave function" ("kinetic part") of the quark self-energy, and one determining the dynamical (constituent) quark mass [14, 25]. Of course, in the case of the quark self-energy the above separation of both sides of the corresponding SDE (quark gap equation) is realized in a direct way, due to the distinct Dirac properties of the two quantities appearing in it, while in the case of the gluon propagator no such straightforward separation is possible. However, an unambiguous way for implementing this separation, which exploited to the fullest the characteristic structure of a certain type of vertices that are inextricably connected with the process of gluon mass generation and naturally appears in the PT-BFM framework, was recently presented in [16].

Specifically, a crucial condition for obtaining out of the SDEs an IR-finite gluon propagator without interfering with the gauge invariance of the theory, is the existence of a set of special vertices that are purely longitudinal and contain massless poles, and must be added to the usual (fully-dressed) vertices of the theory. The role of these vertices is two-fold. On the one hand, thanks to the massless poles they contain, they make possible the emergence of a IR finite solution out of the SDE governing the gluon propagator;

this corresponds essentially to a non-Abelian realization of the well-known Schwinger mechanism [26, 27]. On the other hand, these same poles act like composite Nambu–Goldstone excitations, preserving the form of the STIs of the theory in the presence of a gluon mass.

It turns out that the very nature of these vertices furnishes a solid guiding principle for implementing the aforementioned separation between mass and kinetic terms. In particular, their longitudinal structure, coupled to the fact that one works in the Landau gauge, completely determines the longitudinal component of the mass equation; this is tantamount to knowing the full mass equation, given that the answer is bound to be transverse.

Due to the complexity of the derivation of the equation, we will not discuss it here, but rather sketch its final form as well as its main ingredients, together with the numerical solutions it gives rise to.

Schematically, the equation reads

$$m^2\left(q^2\right) = \alpha_{\rm s}\int\limits_k m^2\left(k^2\right)\left[\mathcal{K}_1(\Delta;q,k) + \alpha_{\rm s}\mathcal{K}_2(\Delta,Y;q,k)\right], \tag{3}$$

where $\mathcal{K}_1$ is the contribution coming form the one-loop dressed diagrams (namely the graphs appearing in the PT-BFM gluon propagator SDE containing trilinear vertices *only*), whereas $\mathcal{K}_2$ is the contribution of two-loop dressed diagrams (that is, the graphs containing quadrilinear vertices). As indicated in Eq. (3), while $\mathcal{K}_1$ contains only the gluon propagator, in $\mathcal{K}_2$ a new form factor Y appears, which involves the three gluon vertex and reads

$$Y\left(k^2\right) = \frac{1}{3k^2}\,k_\alpha g^\delta_\beta \int\limits_\ell \Delta^{\alpha\rho}(\ell)\Delta^{\beta\sigma}(\ell+k)\Gamma_{\sigma\rho\delta}(-\ell-k,\ell,k)\,. \tag{4}$$

The lowest order perturbative calculation of Y (obtained by substituting tree-level values for all quantities appearing in the expression above) yields (after renormalization) $Y \sim \log k^2/\mu^2$; this value multiplied by a constant C (basically modelling, in a rather heuristic way, further corrections that may be added to the "skeleton" provided by the lowest order result) is the one used in [16] for studying numerically the solutions of Eq. (3). The value of C corresponding to the lowest order expression is fixed to the actual value $C = 3\pi C_A\alpha_{\rm s}$; however, it is convenient to treat C as a free parameter, thus disentangling it from the value of $\alpha_{\rm s}$, and studying what happens to the solution spectrum of Eq. (3) when the two parameters are varied independently.

As shown in the left panel of Fig. 3 (where C is now measured in units of $3\pi C_A$), there is a continuous curve formed by the pairs $(C,\alpha_{\rm s})$, for which one finds physical solutions. Indeed, for small values of C one has that no

solution exists; this absence of solutions persists (for the quenched case) until the critical value $\overline{C} \approx 0.56$ is reached, after which one finds exactly one monotonically decreasing solution. However, for values up to $C \approx 0.8$ the coupling needed to get the corresponding running mass is of $\mathcal{O}(1)$, while for the quenched case the expected coupling from the 4-loop (momentum subtraction) calculation is $\alpha_{\rm s} = 0.22$ at $\mu = 4.3$ GeV [28]. This latter value is obtained for $C \approx 1.8$–1.9, whereas for $C \approx 0.88$ one finds the solution to Eq. (3) for the lowest order perturbative value of the coefficient. In general, one observes, as expected, that as C is increased, $\alpha_{\rm s}$ decreases, *e.g.* for $C = 1.1$, 1.3, 1.5 and 1.7 one obtains solutions corresponding to the strong coupling values $\alpha_{\rm s} \approx 0.53$, 0.39, 0.30, and 0.25, respectively.

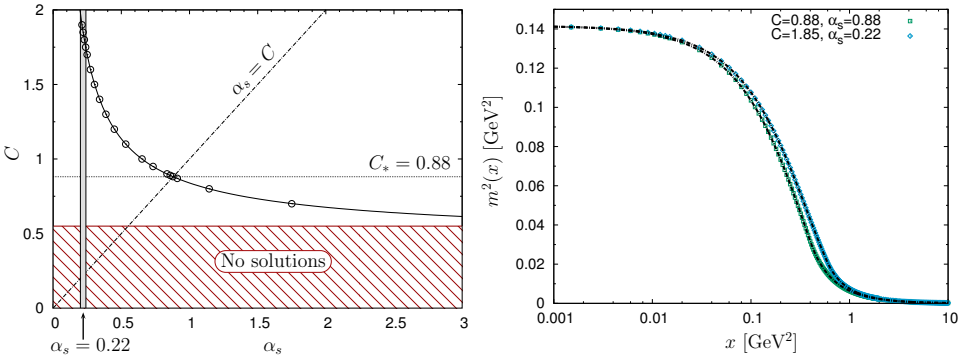


Fig. 3. The curve described by the set of pairs $(C, \alpha_{\rm s})$ for which one finds physical solutions to the full mass equation (3) (left), and the typical monotonically decreasing solution of the mass equation (3) (right).

In the right panel of Fig. 3, we plot the solutions for the most representative C values, *i.e.* $C = 0.88$ and $C = 1.85$ (corresponding to, as already said, $\alpha_{\rm s} \approx 0.88$ and 0.22 respectively), normalized in such a way that the mass at zero coincides with the IR saturating value found in lattice (Landau gauge) quenched simulations [22], or $m^2(0) = \Delta^{-1}(0) \approx 0.141$ GeV^2. As can be readily appreciated, the masses obtained display the basic qualitative features expected on general field-theoretic considerations and employed in numerous phenomenological studies; in particular, they are monotonically decreasing functions of the momentum, and vanish rather rapidly in the ultraviolet [1, 29, 30]. It would seem, therefore, that the PT-BFM all-order analysis described here puts the entire concept of the gluon mass, and a variety of fundamental properties ascribed to it, on a solid first-principle basis.

REFERENCES

[1] J.M. Cornwall, *Phys. Rev.* **D26**, 1453 (1982).
[2] J.M. Cornwall, J. Papavassiliou, *Phys. Rev.* **D40**, 3474 (1989).
[3] D. Binosi, J. Papavassiliou, *Phys. Rev.* **D66**, 111901(R) (2002).
[4] D. Binosi, J. Papavassiliou, *J. Phys. G* **30**, 203 (2004).
[5] D. Binosi, J. Papavassiliou, *Phys. Rep.* **479**, 1 (2009).
[6] L.F. Abbott, *Nucl. Phys.* **B185**, 189 (1981).
[7] A.C. Aguilar, J. Papavassiliou, *J. High Energy Phys.* **12**, 012 (2006).
[8] D. Binosi, J. Papavassiliou, *Phys. Rev.* **D77**, 061702 (2008).
[9] D. Binosi, J. Papavassiliou, *J. High Energy Phys.* **0811**, 063 (2008).
[10] A. Aguilar, D. Binosi, J. Papavassiliou, *Phys. Rev.* **D78**, 025010 (2008).
[11] J. Rodriguez-Quintero, *PoS* **LC2010**, 023 (2010).
[12] M. Pennington, D. Wilson, *Phys. Rev.* **D84**, 119901 (2011).
[13] A. Aguilar, D. Binosi, J. Papavassiliou, *J. High Energy Phys.* **0911**, 066 (2009).
[14] A. Aguilar, J. Papavassiliou, *Phys. Rev.* **D83**, 014013 (2011).
[15] A. Aguilar, D. Binosi, J. Papavassiliou, *Phys. Rev.* **D86**, 014032 (2012).
[16] D. Binosi, D. Ibañez, J. Papavassiliou, `arXiv:1208.1451 [hep-ph]`.
[17] P.A. Grassi, T. Hurth, A. Quadri, *Phys. Rev.* **D70**, 105014 (2004).
[18] J.S. Ball, T.-W. Chiu, *Phys. Rev.* **D22**, 2542 (1980).
[19] D.C. Curtis, M.R. Pennington, *Phys. Rev.* **D42**, 4165 (1990).
[20] A. Kizilersu, M. Pennington, *Phys. Rev.* **D79**, 125020 (2009).
[21] A. Bashir, R. Bermudez, L. Chang, C. Roberts, *Phys. Rev.* **C85**, 045205 (2012).
[22] I. Bogolubsky, E. Ilgenfritz, M. Muller-Preussker, A. Sternbeck, *Phys. Lett.* **B676**, 69 (2009).
[23] A. Ayala *et al.*, `arXiv:1208.0795 [hep-ph]`.
[24] W. Kamleh *et al.*, *Phys. Rev.* **D76**, 094501 (2007).
[25] C.D. Roberts, A.G. Williams, *Prog. Part. Nucl. Phys.* **33**, 477 (1994).
[26] J.S. Schwinger, *Phys. Rev.* **125**, 397 (1962).
[27] J.S. Schwinger, *Phys. Rev.* **128**, 2425 (1962).
[28] P. Boucaud *et al.*, *Phys. Rev.* **D74**, 034505 (2006).
[29] M. Lavelle, *Phys. Rev.* **D44**, 26 (1991).
[30] A.C. Aguilar, J. Papavassiliou, *Eur. Phys. J.* **A35**, 189 (2008).